THE JOURNAL OF PHYSICAL CHEMISTRY C

pubs.acs.org/JPCC Article

Analysis of Exchange Interactions in Dimers of Mn_3 Single-Molecule Magnets, and Their Sensitivity to External Pressure

Jie-Xiang Yu, George Christou, and Hai-Ping Cheng*

Cite This: J. Phys. Chem. C 2020, 124, 14768−14774 Read Online

ACCESS | Metrics & More | Article Recommendations | Supporting Information

ABSTRACT: In light of the potential use of single-molecule magnets (SMMs) in emerging quantum information science initiatives, we report first-principles calculations of the magnetic exchange interactions in $[Mn_3]_2$ dimers of Mn_3 SMMs, connected by covalently attached organic linkers, that have been synthesized and studied experimentally by magnetochemistry and EPR spectroscopy. Energy evaluations calibrated to experimental results give the sign and order of magnitude of the exchange coupling constant (J_{12}) between the two Mn_3 units that match with fits of magnetic susceptibility data and EPR spectra. Wannier function analysis has shown that magnetic interactions can be channeled by oximate groups that have van der Waals interaction and/or by the linkers via covalent bonding of specific systems. Effective tight-binding Hamiltonians are obtained by Hilbert space reduction to include only energy windows near the highest occupied and lowest unoccupied molecular orbitals. Orbital projected spin density of states and alternative Wannier transformations also support this observation. To assess the sensitivity of J_{12} to external pressure, stress−strain curves have been investigated for both hydrostatic and uniaxial pressure, which have revealed a switch of J_{12} from ferromagnetic to antiferromagnetic with increasing pressure.

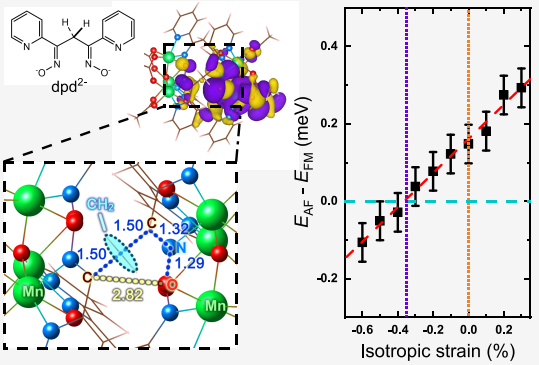

1. INTRODUCTION

Magnetic molecules have stimulated intense interest in chemistry and physics because of their potential applications in quantum information science[1−4] and other future technologies.[5−8] One important class of magnetic molecules are single-molecule magnets (SMMs), which have a sufficiently large anisotropy barrier versus kT to magnetization relaxation that they behave as nanoscale magnets. One of the most investigated properties in SMMs is quantum tunneling of the magnetization vector (QTM) through the anisotropy barrier.[9−13] In dimers of Mn_4 SMMs with S = 9/2 held together by hydrogen-bonding, the resulting weak inter-Mn_4 exchange coupling led to discovery of new phenomena in molecular magnetism, namely (i) exchange-biased QTM whereby the neighboring Mn_4 acted as a bias field shifting the position of the QTM steps in the hysteresis loop,[11] and (ii) the generation of quantum superposition and entanglement states of the two Mn_4 units, which were identified by analysis of the high-frequency electron paramagnetic resonance (EPR) (HF-EPR) spectra.[12] More recently in 2007, triangular $[Mn_3O(O_2CR)_6(py)_3](ClO_4)$ SMMs (R = Me, Et, and Ph) were synthesized containing three ferromagnetically coupled Mn^{III} ions and an S = 6 ground state.[14] Covalent linkage of these Mn_3 SMMs with organic linkers provides a more controlled method than hydrogen-bonding to synthesize a variety of $[Mn_3]_2$ dimers[14] and higher $[Mn_3]_4$ oligomers.[10] The covalent linkage introduces weak exchange coupling between two Mn_3 units in dimers or tetramers, and its sign can be varied depending on the linker identity. These dimers and tetramers were obtained as molecular crystals permitting full structural characterization by X-ray crystallographic studies.

The primary subject of this paper is the $[Mn_3]_2$ dimer with dpd^{2-} linkers (dpd^{2-} = the dianion of 1,3-di(pyridin-2-yl)propane-1,3-dione dioxime), which was found by magnetic susceptibility measurements and HF-EPR spectroscopy to have a ferromagnetic (FM) interaction (J_{12}) between the two Mn_3 units.[14] In addition, HF-EPR was employed to investigate the resulting quantum superposition states in both the crystal and solution phases.[14] The spin Hamiltonian employed was $\hat{H} = \hat{H}_1 + \hat{H}_2 - 2J_{12}\hat{S}_1\cdot\hat{S}_2$ with $\hat{H}_{1,2} = D\hat{S}_{1,2z}{}^2 + g\mu_B\hat{S}\cdot\vec{H}$, where $\hat{S}_{1,2}$ and $\hat{H}_{1,2}$ are the spin and the spin Hamiltonian of each Mn_3 unit 1 and 2, $\hat{S}_z$ is the spin projection along the easy axis, the anisotropy D = −0.22 cm^{-1}, and g_z = 2.00; μ_B is the Bohr magneton and μ_0 is the vacuum permeability. Both the fits of magnetic and EPR data give J_{12} = 0.025 cm^{-1}.

Received: March 12, 2020
Revised: April 27, 2020
Published: June 3, 2020

https://dx.doi.org/10.1021/acs.jpcc.0c02213
J. Phys. Chem. C 2020, 124, 14768−14774

In the absence of theoretical calculations, it was proposed[15] that the Mn d_π magnetic orbitals delocalize into the dpd^{2-} π systems and the J_{12} exchange coupling is propagated by spin polarization of the bonding electrons in the central sp^3 C atom of the linker. Does this explanation give the exact microscopic physics of magnetic exchange in the $[Mn_3]$ dimer? This is the first question we decided to address. The second question is if and how one can tune the J_{12} interaction of a given dimer, and thus the resulting quantum properties. This requires an assessment of the sensitivity of J_{12} to external influences, and an experimentally feasible method to apply external pressure and see how the coupling strength changes. Pressure-dependent investigations have lately become extensively used to uncover new physics behaviors in various materials and states of matter. Particular to magnetic orderings, pressure-dependent structural changes lead to changes in charge and spin ordering, magnetic properties, superconducting transitions,[16,17] and transport behavior in perovskites.[18−21] Specific to molecular magnetic materials, pressure- or strain-dependent studies include enhancing the magnetic ordering temperature in rhenium(IV) molecules,[22] changing steps in quantum tunneling magnetization,[23] and modulating tunneling splitting.[24] It is worthwhile to mention that sometimes "chemical pressure" (ligand-induced perturbation of magnetic cores) is used to modulate magnetic ordering in molecular magnetic systems via altering the volume of solid unit cells.[25,26]

In this paper, we report results from first-principles calculations within the framework of density functional theory (DFT).[27,28] We will show below that our investigations provide electronic and magnetic structures that are necessary for understanding long-range magnetic superexchange interaction, testing the validity of the isolated ion model versus full-crystal models, and providing strain−stress−magnetism relations. Answers to the two questions posted above will fill gaps in current knowledge of SMM clusters and in theoretical modeling, and guide future experiments and the design of new electronic magnetic materials that are pivotal for next generation electronics and technology for quantum information sciences.

2. COMPUTATIONAL METHOD

Our DFT-based calculations are performed with projector augmented wave pseudopotentials[29] implemented in the Vienna Ab initio Simulation Package.[30] The generalized gradient approximation by Perdew, Burke, and Ernzerhof[28] is used as the exchange−correlation energy, and the Hubbard U method[31,32] (U = 2.8 eV, J = 0.9 eV) is applied on Mn(3d) orbitals to include strong-correlation effects. The magnitude of U is determined by the experimental results for the strength of the exchange interaction, corresponding to $E_{AF} - E_{FM}$, the total energy difference between inter-$[Mn_3]$ FM and antiferromagnetic (AFM) spin configurations, of about 0.2 meV per dimer (see Supporting Information for details). An energy cutoff of 600 eV is used for the plane-wave expansion throughout the calculations. The DFT-D3 method with inclusion of van der Waals correction[33] is employed. Total energy, structure optimizing, and electronic structure calculations were performed on three single-molecule $[Mn_3]$-dimers and their ions (we call these gas phase molecules or ions) and one FM dimer in its bulk form. For ions with charge in gas phases, the jellium model is used to keep the whole system charge neutral, and a periodic cubic lattice with a lattice constant of 24.00−30.00 Å is used to keep molecules sufficiently separated in adjacent unit cells. The Γ point only is used for both gas and bulk phases. A 3 × 3 × 3 Γ-centered k-mesh for bulk phases is used for the density-of-state (DOS) calculations. During most structure-optimizing calculations, all forces on each atom are less than 1, or 0.2 meV/Å when external strain is applied. With these criteria, the error of the total energy difference between FM and AFM spin configurations $\delta(E_{AF} - E_{FM})$ is estimated to be about 0.05 meV, which might be reduced further with an energy cutoff larger than 600 eV. After we obtain the eigenstates and eigenvalues, a unitary transformation of Bloch waves is performed to construct the tight-binding Hamiltonian in a Wannier function (WF) basis by using the maximally localized WF (MLWF) method[34] implemented in the Wannier90 package.[35] The WF-based Hamiltonian has the same exact eigenvalues as those obtained by DFT calculations within an inner energy window. For periodic systems, an outer window is often needed to disentangle the Bloch states.[36]

3. RESULTS AND DISCUSSION

3.1. Geometries of $[Mn_3]_2$ Dimers. The structures of three SMM $[Mn_3]_2$ dimers are shown in Figure 1, where two

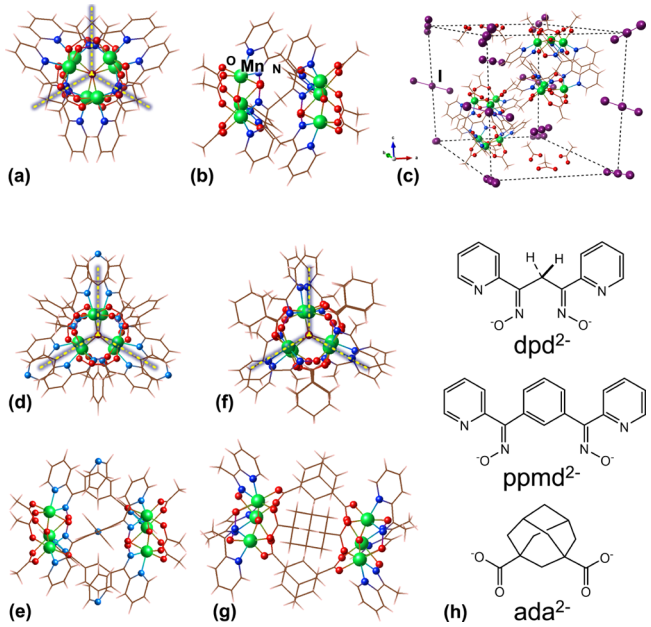

Figure 1. Structure of $([Mn_3]_2\text{-}(dpd)_3)^{2+}$ in (a,b) the gas phase and (c) the crystal phase. Structure of the (d) (e) $([Mn_3]_2\text{-}(ppmd)_3)^{2+}$ and (f,g) $([Mn_3]_2\text{-}(ada)_3)^{2+}$ molecules. (h) Structure of the linkers. Color code: Mn green, O red, N blue, and I purple. Guidelines show the C_3 symmetry.

$Mn_3O(O_2CMe)_3$ units are linked covalently by three different linkers. Each $[Mn_3]$ unit has C_3 symmetry and a S = 6 spin ground state from FM coupling of its three Mn^{3+} ions (each S = 2). In the resulting dimer, the two Mn_3 triangular planes are parallel. The dimer with the shortest linker is $([Mn_3]_2\text{-}(dpd)_3)^{2+}$; the dpd^{2-} linker consists of two oximate groups connected to a central CH_2 group (Figure 1h). For this system, we investigated its crystalline phase as well as individual dimers in isolation. According to experiment,[15] the molecular crystal phase of the $([Mn_3]_2\text{-}(dpd)_3)^{2+}$ dimer has space group $P\bar{3}1c$ with trigonal symmetry in the hexagonal lattice. Each unit cell contains two dimers, which are parallel. The counterions of the $([Mn_3]_2\text{-}(dpd)_3)^{2+}$ dimer are two I_3^- anions, so that each unit

https://dx.doi.org/10.1021/acs.jpcc.0c02213
J. Phys. Chem. C 2020, 124, 14768−14774

cell contains four I_3^-. Structure optimization was performed with experimental lattice constants a = 16.569 Å, c = 18.285 Å; Figure 1c shows the optimized atomic structure of $([Mn_3]_2$-$(dpd)_3)_2(I_3)_4$, even though experimental studies could not determine the location and orientation of the I_3^- counter ions.

3.2. lElectronic Structures of $[Mn_3]_2$ Dimers. The calculated ground state of the isolated (gas phase) $([Mn_3]_2$-$(dpd)_3)^{2+}$ dimer has spin equal to 12, with each $[Mn_3]$ monomer in a S = 6 spin state (magnetic moment = 12 μ_B). Figure 2a,b shows the total DOS and projected DOS (PDOS)

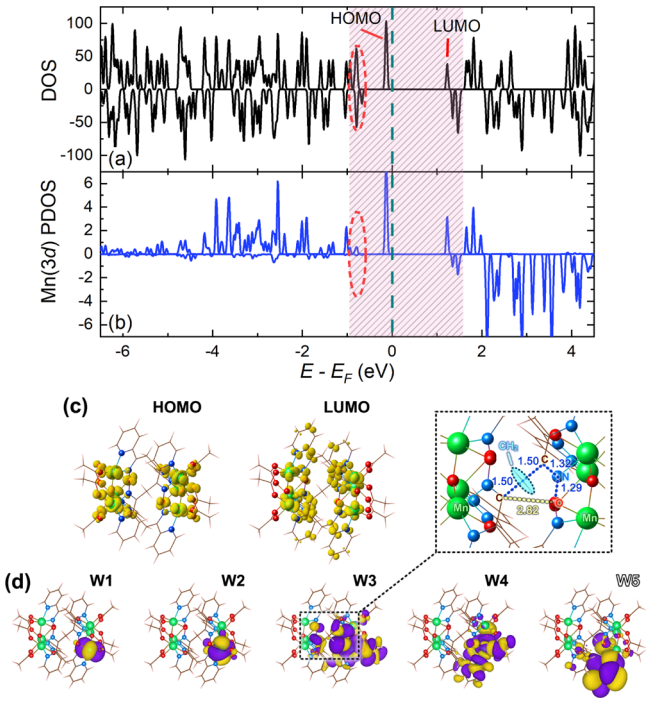

Figure 2. Electronic structure for the gas phase of $([Mn_3]_2$-$(dpd)_3)^{2+}$ dimers. (a) The total DOS and (b) orbit-resolved PDOS of the Mn(3d) orbitals. Positive and negative values correspond to spin-majority and spin-minority channels, respectively. The Fermi level is set to zero. The HOMO and LUMO are labeled; the marked state refers to the sub-HOMO state with a few Mn(3d) components; the shadow region refers to the inner energy window for the MLWF. (c) Partial charge density of the HOMO (left) and the LUMO (right). (d) Aligned by on-site energies, five WFs in the spin-majority channel centered on the same Mn atom. Solid and hollow labels represent occupied and unoccupied WFs, respectively.

of the Mn(3d) orbitals. The gap between the highest occupied molecular orbital (HOMO) and the lowest unoccupied molecular orbital (LUMO) is 1.2 eV. The isosurfaces of HOMO and LUMO partial charge density shown in Figure 2c are all in the spin-majority or spin-up channel, and both are dominated by the Mn(3d) orbitals. However, just below the HOMO, the states circled by red-dashed lines (Figure 2a,b) have a few features of Mn(3d).

The inter-Mn_3 magnetic interaction is weak but long-range. To understand the states near the HOMO and LUMO and how they affect the inter-Mn_3 exchange interaction, we performed MLWF calculations to obtain the WF-based Hamiltonian using the inner energy window shown in Figure 2a,b, with Mn(3d) orbitals as the initial projections (or basis function) of WFs for reducing the dimensionality of Hilbert space (or downfolding in condensed matter literature) process. Figure 2d shows the five WFs in the spin-majority channel with the basis function concentrated on one Mn atom. The two WFs, W1 and W2, with lowest on-site energies about −3.0 eV relative to the Fermi level in the DOS, are just localized on Mn. Three other WFs, W3 to W5 with higher on-site energies, however, have significant contributions from the dpd^{2-} oximate groups and acetate ligands indicating that the sub-HOMO states are dominated by ligand orbitals. More discussion about ligands is included in the Supporting Information Considering the S = 2 spin state of Mn with four unpaired 3d electrons, W5 with the highest on-site energy is the only unoccupied WF in this WF basis. Other WFs centered on other Mn atoms have similar behaviors, so that W1 to W5 can be regarded as five groups to classify the thirty total WFs in the Hamiltonian. The strongest hopping t in the Hamiltonian between WFs belonging to different sides of the dimer is about 0.070 eV. It comes from one W3-like occupied WF at one side of the dimer and one W5-like unoccupied WF at the other side. Note that the overlap between W3 and W5 is dominated by two dpd^{2-} oximate groups (one from each Mn_3 unit) instead of central CH_2 units and the energy level for the central dpd^{2-} C atom is far below the HOMO (See Figure S1a in Supporting Information). Because the closet interatomic distance between oximate groups on different sides is 2.53 Å and an O−C contact between the two groups is 2.85 Å (part of the spin-coupling path), which is in the region of van der Waals interaction, the J_{12} exchange interaction in this system likely has its major contribution from channels in which a van der Waals contact between oximate groups plays a role. Magnetic coupling via van der Waals interaction is a subject of great current interest.[37] Detailed analysis shows that all six paths represented by two sets of W3−W5 (one each side) contribute to the overall coupling, J_{12}. The electronic structure of the bulk phase $([Mn_3]_2$-$(dpd)_3)_2(I_3)_4$ has also been investigated. The FM spin configuration shows that the total spin in one unit cell is S = 24 with magnetic moment 48 μ_B, so that each $[Mn_3]$ monomer still has a S = 6 spin state with magnetic moment 12.0 μ_B, indicating the same valence state of the $([Mn_3]_2$-$(dpd)_3)^{2+}$ cation as that in the gas phase.

For the other two $[Mn_3]$ dimers, experiments found that $([Mn_3]_2$-$(ada)_3)^{2+}$ has AFM coupling between the two $[Mn_3]$ units, while the inter-Mn_3 coupling in $([Mn_3]_2$-$(ppmd)_3)^{2+}$ is FM. Our total energy calculations for both of them show that $E_{AF} - E_{FM}$ for $([Mn_3]_2$-$(ada)_3)^{2+}$ is −0.02 meV per dimer and that for $([Mn_3]_2$-$(ppmd)_3)^{2+}$ is 0.03 meV per dimer. These results for $|E_{AF} - E_{FM}|$ are one order smaller than that for $([Mn_3]_2$-$(dpd)_3)^{2+}$ and are within our numerical error. However, we can still obtain insight into electronic structure and exchange pathways. The tiny inter-Mn_3 exchange can be explained by the electronic structure. Figure 3a,b shows the total DOS and PDOS of the Mn(3d) orbitals for $([Mn_3]_2$-$(ppmd)_3)^{2+}$ dimers. The DOS and PDOS are very similar to those for $([Mn_3]_2$-$(dpd)_3)^{2+}$, where the HOMO and LUMO are dominated by the Mn(3d) orbitals and the sub-HOMOs do not have features of Mn(3d). The atom-centered WFs for the tight-binding Hamiltonian for $([Mn_3]_2$-$(ppmd)_3)^{2+}$ [Figure 3c] are also similar to those in $([Mn_3]_2$-$(dpd)_3)^{2+}$, where two localized WFs have lower on-site energies, and three other WFs with higher on-site energies have some features of the acetate ligand O_2CMe but mostly the linker ppmd, indicating that the linkers are responsible for the exchange couplings. In the WF basis for $([Mn_3]_2$-$(ppmd)_3)^{2+}$, W5 with the highest on-site energy is unoccupied. Among all the inter-Mn_3 hopping in

https://dx.doi.org/10.1021/acs.jpcc.0c02213
J. Phys. Chem. C 2020, 124, 14768−14774

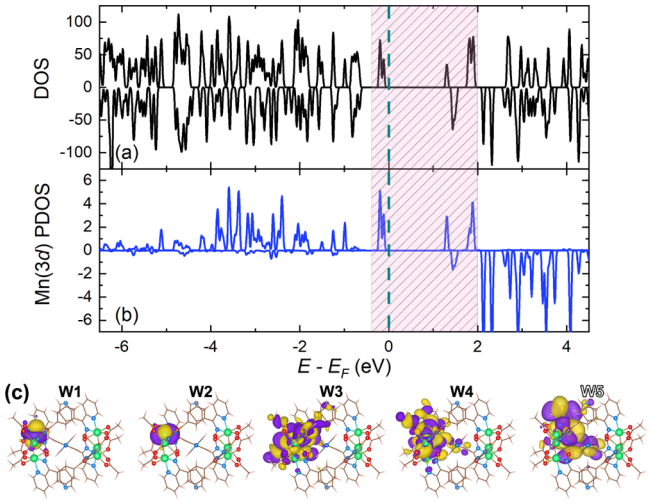

Figure 3. Electronic structure for the gas phase of $([Mn_3]_2$-$(ppmd)_3)^{2+}$ dimers. (a) The total DOS and (b) PDOS of the Mn(3d) orbitals. The shadow region refers to the inner energy window for the MLWF. (c) Ordered by on-site energies, five WFs in the spin-majority channel centered on the same Mn atom. Solid/hollow labels represent occupied and unoccupied WFs respectively.

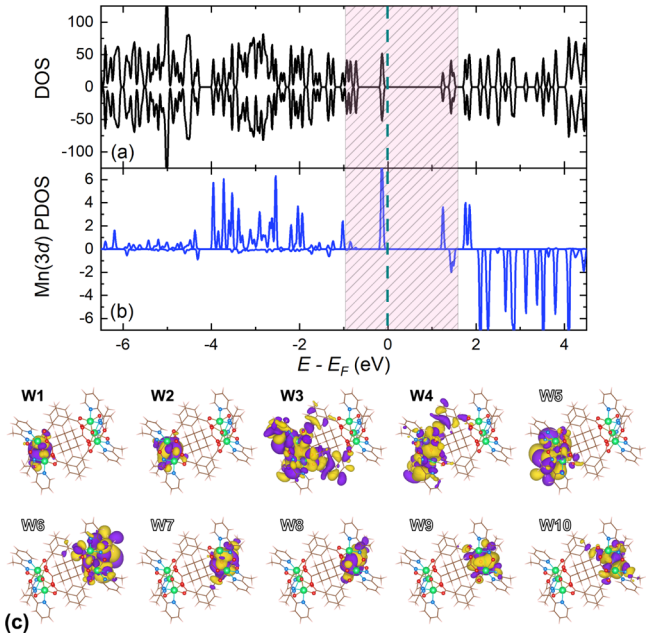

Figure 4. Electronic structure for the gas phase of $([Mn_3]_2$-$(ada)_3)^{2+}$ dimers with AFM spin ordering. (a) The total DOS and (b) PDOS of the Mn(3d) orbitals. The shadow region refers to the inner energy window for the MLWF. (c) In the spin-majority channel, 10 WFs, of which five are centered on an Mn atom at one side of the dimer and the other five centered on the corresponding Mn atom at the other side. These WFs are ordered by on-site energies, and solid/hollow labels represent occupied/unoccupied WFs, respectively.

the Hamiltonian, the strongest hopping t between occupied and unoccupied WFs is −0.016 eV, which again comes from the hopping between the occupied W3-like WF and the unoccupied W5-like WF. Thus, $([Mn_3]_2$-$(ppmd)_3)^{2+}$ has much weaker inter-Mn_3 hopping. Linker $ppmd^{2-}$ with a larger size than dpd^{2-} makes weaker both the hopping across the linker and the overall exchange through van der Waals contacts and spin polarization effects. Numerically, the strength of the exchange interaction, which is usually proportional to t^2 for $([Mn_3]_2$-$(ppmd)_3)^{2+}$ is about one order of magnitude smaller than that for $([Mn_3]_2$-$(dpd)_3)^{2+}$, consistent with the total energy results.

The DOS results for AFM $([Mn_3]_2$-$(ada)_3)^{2+}$ are shown in Figure 4a,b. Because of AFM spin-ordering, the total DOS are identical in both spin channels. The PDOS on one Mn still gives the S = 2 high-spin state, the same as that for the other two dimers. The atomic-centered WFs for the tight-binding Hamiltonian are also obtained. Note that for this dimer, the two Mn_3 units are exchange-coupled only through the covalent linkers. In the same spin channel, Figure 4c gives ten WFs, with five of them, W1 to W5, centered on a Mn atom at one side of the dimer and the other five, W6 to W10, centered on the corresponding Mn atom at the other side. That means, W1 to W5 are the spin-up atomic-like orbitals of one Mn and W6 to W10 are the spin-down atomic-like orbitals of another. Because of S = 2 high-spin state of Mn with four unpaired 3d electrons, the four WFs, W1 to W4, with the lowest energies are occupied in this tight-binding basis and others are unoccupied. Among the occupied WFs, W1 and W2 are localized on Mn while W3 and W4 have a comparatively significant contribution from the ada linkers. Among the unoccupied WFs at the other side of the dimer, all WFs except for W6 are localized on Mn. The strongest inter-monomer hopping t in the Hamiltonian between occupied and unoccupied WFs is −0.015 eV between W3 and W10. The value of t^2 is only one-twentieth of that in $([Mn_3]_2$-$(dpd)_3)^{2+}$. Considering that the only difference between $([Mn_3]_2$-$(dpd)_3)^{2+}$ and $([Mn_3]_2$-$(ada)_3)^{2+}$ is the different linkers, which affect the strength of inter-Mn_3 hopping, we can estimate that the strength of the exchange interaction of $([Mn_3]_2$-$(ada)_3)^{2+}$ is one-twentieth in magnitude of that in $([Mn_3]_2$-$(dpd)_3)^{2+}$, numerically consistent with the total energy results.

3.3. Strain-Induced Magnetic Transition. Although HF-EPR experiments[15] have shown that covalently linked $[Mn_3]_2$ dimers remain intact in the solution phase and retain their J_{12} exchange coupling and resulting quantum superposition states, their low Young's modulus in the solid phase suggests a nontrival strain-sensitive response. To study the strain response of the J_{12} magnetic interaction, we applied external strain on $([Mn_3]_2$-$(dpd)_3)_2(I_3)_4$ by changing the lattice constant. Figure 5a,b shows the isotropic strain-dependent results. The value of $E_{AF} - E_{FM}$ as a function of strain shows that the magnetic interaction can transition from FM to AFM when a compressive strain of about 0.4% in length, or 1.2% in volume, is applied. The hydrostatic pressure corresponding to this transition is about 0.06 GPa according to Figure 5b. This strain-induced FM−AFM transition can also occur with a uniaxial strain by changing the out-of-plane lattice constant c and keeping the volume of the unit cell invariant. According to the results shown in Figure 5d,e, the sign of $E_{AF} - E_{FM}$ shifts from positive to negative when c is changed by about 1.4%; the corresponding compressive pressure in that direction is also about 0.06 GPa.

Because the $[Mn_3]$-dimer is linked covalently by the linker dpd^{2-}, the mechanism of the magnetic interaction is dominated by superexchange, which is sensitive to both the bond length and bond angle. Figure 5c shows the distance between two $[Mn_3]$ planes and the C−C−C bond angle of the linker dpd as a function of strain. As both isotropic and uniaxial compressive strains increase, the magnitude of the bond angle

https://dx.doi.org/10.1021/acs.jpcc.0c02213
J. Phys. Chem. C 2020, 124, 14768−14774

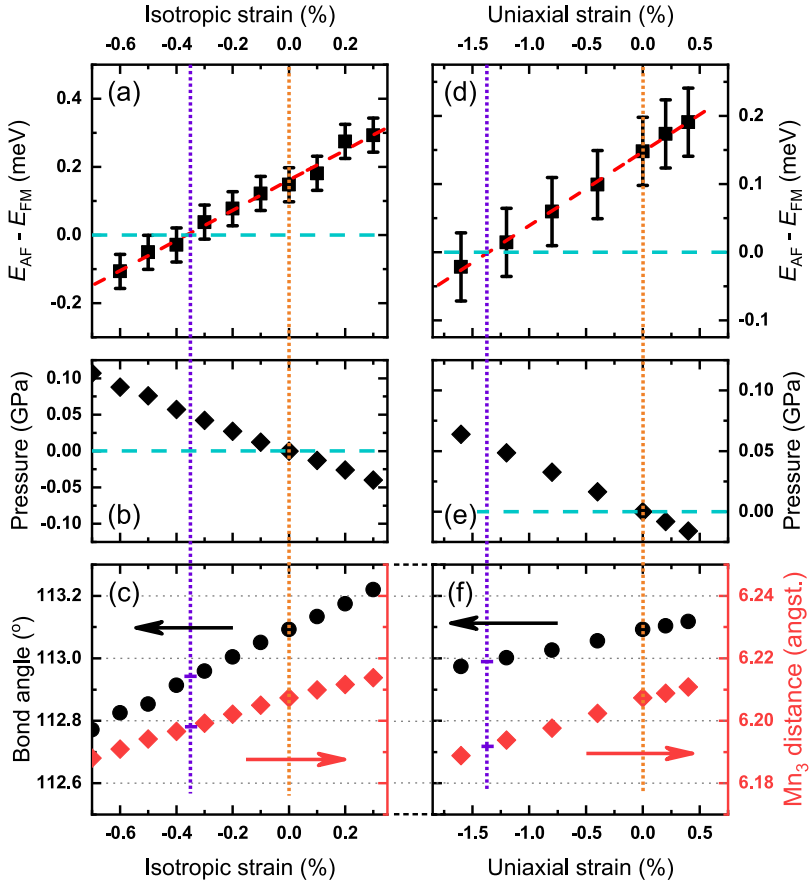

Figure 5. Strain dependences for $([Mn_3]_2\text{-}(dpd)_3)_2(I_3)_4$ bulk. (a) Energy difference $E_{AF} - E_{FM}$ per dimer, (b) pressure, (c) C−C−C bond angle (black dots) of the linker (dpd) and distance (red dots) between two $[Mn_3]$ as a function of isotropic strain. (d−f) Similar results as a function of uniaxial strain, (c,f) share the same vertical scales. Violet and orange vertical-dotted lines represent FM/AF transitions and the unstrained results, respectively.

and the distance decreases with an almost linear relation. At the transition point, the distance between two $[Mn_3]$ planes is 6.198 Å under isotropic strain, 0.14% closer than the zero pressure value. The number under uniaxial strain is 6.192 Å, 0.24% closer than the zero-pressure case. On the other hand, the C−C−C bond angle of the linker dpd is 112.94°, 0.13% smaller than for zero pressure. The number under uniaxial strain is 112.99°, 0.09% smaller than zero pressure. The percentage of the change of both distances and bond angles is much smaller than the percentage of the applied strain, indicating that the major response to strain is the changing of intermolecular distances instead of the modification of the bond lengths and angles within one $[Mn_3]$-dimer molecule. However, this small change is enough to drive the FM−AFM transition, reflecting the sensitivity of the response to the magnetic exchange interaction and confirming the super-exchange feature.

4. CONCLUSION

In summary, we have studied the electronic and magnetic properties of a series of SMM $[Mn_3]_2$ dimers based on the first-principles calculations. While energetic determination of the magnetic order of dimers relies on experiments because of the weak coupling nature, the coupling pathway can be uncovered by Wannier orbital analysis. Total DOS and PDOS results show similar electronic structures of Mn(3d) orbitals among the three dimers. By downfolding into a Mn-centered WF basis, the tight-binding Hamiltonian indicates that only $([Mn_3]_2\text{-}(dpd)_3)^{2+}$ has significant inter-Mn_3 hopping via oximate groups sufficient to bring about a significant exchange coupling contribution. The other two $[Mn_3]$-dimers, $([Mn_3]_2\text{-}(ppmd)_3)^{2+}$ and $([Mn_3]_2\text{-}(ada)_3)^{2+}$, have small hopping coefficients, via covalently bonded linkers, leading to a much weaker exchange interaction. These results suggest that, like linkers, van der Waals contacts between ligands can also affect the sign and strength of magnetic exchange. The calculated results also show that even though the isolated dimer model is different in structure from the bulk form, the trends in the relative energies and densities of states are the same. It is a reasonable model for WF analysis. Finally, the strain dependence of magnetic interactions in the bulk phase of $([Mn_3]_2\text{-}(dpd)_3)_2(I_3)_4$ is investigated under both hydrostatic and uniaxial pressure. A strain-induced FM−AFM transition is identified when an external pressure of about 0.06 GPa is applied, indicating the sensitivity of the response to magnetic exchange interaction and providing potential application to molecular-based spintronics. Experimental work on pressure dependence is underway.

■ ASSOCIATED CONTENT

Supporting Information

The Supporting Information is available free of charge at https://pubs.acs.org/doi/10.1021/acs.jpcc.0c02213.

https://dx.doi.org/10.1021/acs.jpcc.0c02213
J. Phys. Chem. C 2020, 124, 14768−14774

Details of U-dependent calculations, WF-based tight-binding Hamiltonian, and other density-of-state results (PDF)

AUTHOR INFORMATION

Corresponding Author

Hai-Ping Cheng − *Department of Physics and The M2QM Center, University of Florida, Gainesville, Florida 32611-7011, United States*; Email: hping@ufl.edu

Authors

Jie-Xiang Yu − *Department of Physics, The M2QM Center, and The Quantum Theory Project, University of Florida, Gainesville, Florida 32611-7011, United States*; orcid.org/0000-0002-3739-3253

George Christou − *The M2QM Center and Department of Chemistry, University of Florida, Gainesville, Florida 32611-7011, United States*; orcid.org/0000-0001-5923-5523

Complete contact information is available at: https://pubs.acs.org/10.1021/acs.jpcc.0c02213

Notes

The authors declare no competing financial interest.

ACKNOWLEDGMENTS

This work was supported as part of the Center for Molecular Magnetic Quantum Materials, an Energy Frontier Research Center funded by the U.S. Department of Energy, Office of Science, Basic Energy Sciences under Award no. DE-SC0019330. Computations were performed at NERSC and UFRC.

REFERENCES

(1) Leuenberger, M. N.; Loss, D. Quantum Computing in Molecular Magnets. *Nature* **2001**, *410*, 789−793.

(2) Gaita-Ariño, A.; Luis, F.; Hill, S.; Coronado, E. Molecular Spins for Quantum Computation. *Nat. Chem.* **2019**, *11*, 301−309.

(3) Ding, Y. S.; Yu, K. X.; Reta, D.; Ortu, F.; Winpenny, R. E. P.; Zheng, Y. Z.; Chilton, N. F. Field- and Temperature-Dependent Quantum Tunnelling of the Magnetisation in a Large Barrier Single-Molecule Magnet. *Nat. Commun.* **2018**, *9*, 10.

(4) von Kugelgen, S.; Freedman, D. E. A Chemical Path to Quantum Information. *Science* **2019**, *366*, 1070−1071.

(5) Hymas, K.; Soncini, A. Molecular Spintronics Using Single-Molecule Magnets under Irradiation. *Phys. Rev. B: Condens. Matter Mater. Phys.* **2019**, *99*, 245404.

(6) Bogani, L.; Wernsdorfer, W. Molecular Spintronics Using Single-Molecule Magnets. *Nat. Mater.* **2008**, *7*, 179−186.

(7) Wernsdorfer, W.; Bhaduri, S.; Tiron, R.; Hendrickson, D. N.; Christou, G. Spin-Spin Cross Relaxation in Single-Molecule Magnets. *Phys. Rev. Lett.* **2002**, *89*, 197201.

(8) Wu, Y.-N.; Zhang, X. G.; Cheng, H.-P. Giant Molecular Magnetocapacitance. *Phys. Rev. Lett.* **2013**, *110*, 217205.

(9) Thomas, L.; Lionti, F.; Ballou, R.; Gatteschi, D.; Sessoli, R.; Barbara, B. Macroscopic Quantum Tunnelling of Magnetization in a Single Crystal of Nanomagnets. *Nature* **1996**, *383*, 145−147.

(10) Nguyen, T. N.; Wernsdorfer, W.; Abboud, K. A.; Christou, G. A Supramolecular Aggregate of Four Exchange-Biased Single-Molecule Magnets. *J. Am. Chem. Soc.* **2011**, *133*, 20688−20691.

(11) Aubin, S. M. J.; Sun, Z.; Pardi, L.; Krzystek, J.; Folting, K.; Brunel, L.-C.; Rheingold, A. L.; Christou, G.; Hendrickson, D. N. Reduced Anionic Mn-12 Molecules with Half-Integer Ground States as Single-Molecule Magnets. *Inorg. Chem.* **1999**, *38*, 5329−5340.

(12) Gatteschi, D.; Sessoli, R. Quantum Tunneling of Magnetization and Related Phenomena in Molecular Materials. *Angew. Chem. Int. Ed.* **2003**, *42*, 268−297.

(13) Guo, Y.-N.; Xu, G.-F.; Wernsdorfer, W.; Ungur, L.; Guo, Y.; Tang, J.; Zhang, H.-J.; Chibotaru, L. F.; Powell, A. K. Strong Axiality and Ising Exchange Interaction Suppress Zero-Field Tunneling of Magnetization of an Asymmetric Dy-2 Single-Molecule Magnet. *J. Am. Chem. Soc.* **2011**, *133*, 11948−11951.

(14) Stamatatos, T. C.; Foguet-Albiol, D.; Lee, S.-C.; Stoumpos, C. C.; Raptopoulou, C. P.; Terzis, A.; Wernsdorfer, W.; Hill, S. O.; Perlepes, S. P.; Christou, G. "Switching on" the Properties of Single-Molecule Magnetism in Triangular Manganese(Iii) Complexes. *J. Am. Chem. Soc.* **2007**, *129*, 9484−9499.

(15) Nguyen, T. N.; Shiddiq, M.; Ghosh, T.; Abboud, K. A.; Hill, S.; Christou, G. Covalently Linked Dimer of Mn-3 Single-Molecule Magnets and Retention of Its Structure and Quantum Properties in Solution. *J. Am. Chem. Soc.* **2015**, *137*, 7160−7168.

(16) Torikachvili, M. S.; Bud'ko, S. L.; Ni, N.; Canfield, P. C. Pressure Induced Superconductivity in Cafe(2)as(2). *Phys. Rev. Lett.* **2008**, *101*, 057006.

(17) Kimura, N.; Ito, K.; Saitoh, K.; Umeda, Y.; Aoki, H.; Terashima, T. Pressure-Induced Superconductivity in Noncentrosymmetric Heavy-Fermion Cerhsi3. *Phys. Rev. Lett.* **2005**, *95*, 247004.

(18) Radaelli, P. G.; Iannone, G.; Marezio, M.; Hwang, H. Y.; Cheong, S.-W.; Jorgensen, J. D.; Argyriou, D. N. Structural Effects on the Magnetic and Transport Properties of Perovskite $A_{1-x}A'_xMnO_3$ (x=0.25, 0.30). *Phys. Rev. B: Condens. Matter Mater. Phys.* **1997**, *56*, 8265−8276.

(19) Moritomo, Y.; Kuwahara, H.; Tomioka, Y.; Tokura, Y. Pressure Effects on Charge-Ordering Transitions in Perovskite Manganites. *Phys. Rev. B: Condens. Matter Mater. Phys.* **1997**, *55*, 7549−7556.

(20) Trimarchi, G.; Binggeli, N. Structural and Electronic Properties of Lamno3 under Pressure: An ab initio LDA+U Study. *Phys. Rev. B: Condens. Matter Mater. Phys.* **2005**, *71*, 035101.

(21) Pinsard-Gaudart, L.; Rodriguez-Carvajal, J.; Daoud-Aladine, A.; Goncharenko, I.; Medarde, M.; Smith, R. L.; Revcolevschi, A. Stability of the Jahn-Teller Effect and Magnetic Study of $LaMnO_3$ under Pressure. *Phys. Rev. B: Condens. Matter Mater. Phys.* **2001**, *64*, 064426.

(22) Woodall, C. H.; et al. Pressure Induced Enhancement of the Magnetic Ordering Temperature in Rhenium(IV) Monomers. *Nat. Commun.* **2016**, *7*, 7.

(23) Atkinson, J. H.; Fournet, A. D.; Bhaskaran, L.; Myasoedov, Y.; Zeldov, E.; del Barco, E.; Hill, S.; Christou, G.; Friedman, J. R. Effects of Uniaxial Pressure on the Quantum Tunneling of Magnetization in a High-Symmetry Mn-12 Single-Molecule Magnet. *Phys. Rev. B: Condens. Matter Mater. Phys.* **2017**, *95*, 11.

(24) Foss-Feig, M. S.; Friedman, J. R. Geometric-Phase-Effect Tunnel-Splitting Oscillations in Single-Molecule Magnets with Fourth-Order Anisotropy Induced by Orthorhombic Distortion. *Eur. Phys. Lett.* **2009**, *86*, 27002.

(25) Seikh, M. M.; Caignaert, V.; Perez, O.; Raveau, B.; Hardy, V. Interplay between Single-Ion Magnetism, Single-Chain Magnetism and Long-Range Ordering in the Spin Chain Oxides $Sr_{4-x}Ca_xMn_2CoO_9$. *J. Mater. Chem. C* **2018**, *6*, 3362−3372.

(26) Cao, T. S.; Chen, D.-T.; Abboud, K. A.; Zhang, X. G.; Cheng, H.-P.; Christou, G. Feasibility of Ground State Spin Switching in a Molecular Analogue of the Mixed-Metal Oxides with the Perovskite Structure. *Polyhedron* **2019**, *176*, 114275.

(27) Kohn, W.; Sham, L. J. Self-Consistent Equations Including Exchange and Correlation Effects. *Phys. Rev.* **1965**, *140*, A1133−A1138.

(28) Perdew, J. P.; Burke, K.; Ernzerhof, M. Generalized Gradient Approximation Made Simple. *Phys. Rev. Lett.* **1996**, *77*, 3865−3868.

(29) Blöchl, P. E. Projector Augmented-Wave Method. *Phys. Rev. B: Condens. Matter Mater. Phys.* **1994**, *50*, 17953.

(30) Furthmüller, K. a. J. *Vasp*; VASP Institut für Materialphysik, Universität Wien: Vienna, Austria, 1999.

(31) Liechtenstein, A. I.; Anisimov, V. I.; Zaanen, J. Density-Functional Theory and Strong-Interactions - Orbital Ordering in

Mott-Hubbard Insulators. *Phys. Rev. B: Condens. Matter Mater. Phys.* **1995**, *52*, R5467−R5470.
(32) Vaugier, L.; Jiang, H.; Biermann, S.; Hubbard, U.; Hund Exchange, J. Transition Metal Oxides: Screening Versus Localization Trends from Constrained Random Phase Approximation. *Phys. Rev. B: Condens. Matter Mater. Phys.* **2012**, *86*, 165105.
(33) Grimme, S.; Antony, J.; Ehrlich, S.; Krieg, H. A Consistent and Accurate Ab Initio Parametrization of Density Functional Dispersion Correction (Dft-D) for the 94 Elements H-Pu. *J. Chem. Phys.* **2010**, *132*, 154104.
(34) Marzari, N.; Vanderbilt, D. Maximally Localized Generalized Wannier Functions for Composite Energy Bands. *Phys. Rev. B: Condens. Matter Mater. Phys.* **1997**, *56*, 12847−12865.
(35) Mostofi, A. A.; Yates, J. R.; Lee, Y.-S.; Souza, I.; Vanderbilt, D.; Marzari, N. Wannier90: A Tool for Obtaining Maximally-Localised Wannier Functions. *Comput. Phys. Commun.* **2008**, *178*, 685−699.
(36) Zhang, L.; Staar, P.; Kozhevnikov, A.; Wang, Y. P.; Trinastic, J.; Schulthess, T.; Cheng, H. P. DFT Plus Dmft Calculations of the Complex Band and Tunneling Behavior for the Transition Metal Monoxides Mno, Feo, Coo, and Nio. *Phys. Rev. B: Condens. Matter Mater. Phys.* **2019**, *100*, 035104.
(37) Li, T.; et al. Pressure-Controlled Interlayer Magnetism in Atomically Thin Cri3. *Nat. Mater.* **2019**, *18*, 1303.

https://dx.doi.org/10.1021/acs.jpcc.0c02213
J. Phys. Chem. C 2020, 124, 14768−14774